Journal of Materials Chemistry A

Accepted Manuscript

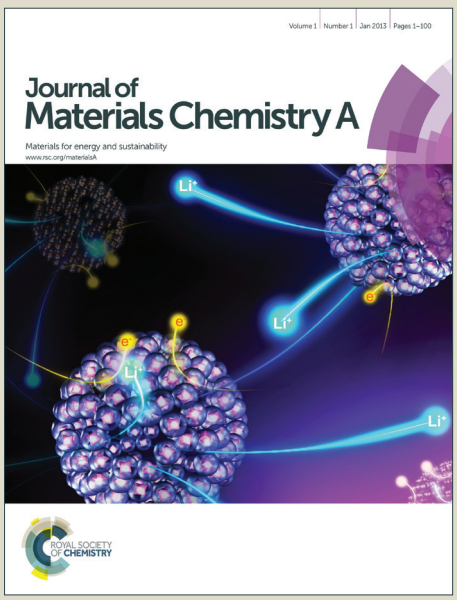

ROYAL SOCIETY OF CHEMISTRY

www.rsc.org/materialsA

Journal Name

COMMUNICATION

Ionic Block Copolymer Doped Reduced Graphene Oxide Supports with Ultra-fine Pd Nanoparticles: Strategic Realization of Ultra-accelerated Nanocatalysis

Received 00th January 20xx,
Accepted 00th January 20xx

DOI: 10.1039/x0xx00000x

www.rsc.org/

Kie Yong Cho,[a,b] Yong Sik Yeom,[a] Heun Young Seo,[a] Pradip Kumar,[b] Albert S. Lee,[b] Kyung-Youl Baek[b,c] and Ho Gyu Yoon[a,*]

We synthesized an ultra-fine Pd nanocatalyst supported by ionic block copolymer doped reduced graphene oxide (Pd-PIBrGO) for ultra-accelerated nanocatalysis. This hybrid catalyst exhibited exceptionally advanced catalytic performance for the reduction of methylene blue using miniscule quantities of the Pd-PIBrGO due to facilated diffusion of the reagents, resulting in full reduction within a few seconds, showing a 280-fold increase of the rate constant over Pd-rGO without ionic block copolymer.

Metal nanoparticles (NPs) have been rigorously investigated as catalysts because of their nanometer-size, which provides large surface areas, unique morphologies, and high catalytic performance.[1-3] Despite their enormous catalytic advantages, the catalytic activity of metal NPs is hampered by formidable drawbacks due to the instability and facile aggregation of NPs, which are potentially detrimental to the catalytic performance.[4]

In the past decade, the aforementioned limitations have been overcome by introducing supports to stabilize the metal NPs by impeding mass aggregation and to enhance the recyclability using carbon nanomaterials, metal oxides, functional polymers, and their hybrids.[5-8] Among the various supports, graphene-based carbon materials with chemical modifications and/or polymeric additives have received significant attention for catalytic applications because of their unique morphological characteristics. These characteristics result in a large area for interaction with metal NPs and reagents, easy accessibility, dimensional stability, and amenability to further modifications.[9,10] Particularly, chemical modification of graphene-based carbon materials and combination of these species with functional polymers for hybridization with metal NPs have been successfully utilized to achieve notable enhancement of the catalytic activity, owing to enhanced structural stability, diffusivity to the active metal catalyst, and morphological effects.[11-18] For instance, Li et al. reported the application of graphene-functionalized with hyper-branched polymers hybridized with Au NPs as a catalyst for the reduction of 4-nitrophenol (4-NP) to 4-aminophenol (4-AP).[19] This Au NP-containing hybrid material exhibited enhanced catalytic performance with a higher reaction rate constant (k = 0.59 min^{-1}) than Au NP without the graphene support (k = 0.31 min^{-1}). Although the support effects facilitate significant enhancement of the catalytic performance, exceptional enhancement still remains possible via strategies such as hybridization of the support with ultra-fine particles (1–3 nm), dense decoration, and good dispersion of the metal NPs, as well as by inducing effective diffusion of reagents to the active metal catalyst. This enhancement is possible because these morphological factors can also lead to increased surface to volume ratio (S/V), high density of edges and corner atoms, and adequate accessibility of reagents.

In this communication, pyrene-functionalized ionic block copolymer (PIB)-doped reduced graphene oxide (rGO) is utilized as a support (PIBrGO) for hybridization with Pd NPs by using a facile in-situ process, resulting in highly dense

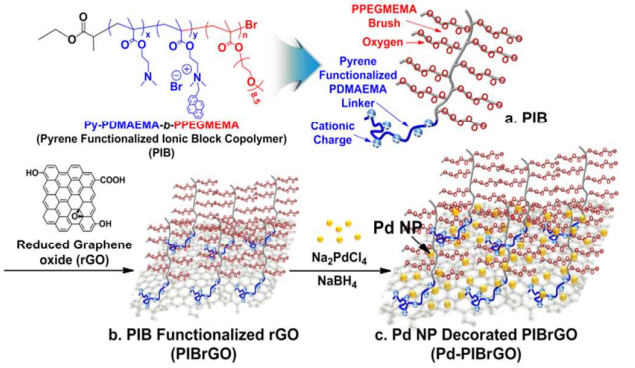

Fig. 1 Schematic depiction of the preparation of Pd NP decorated PIBrGO hybrid nanocomposites.

[a] *Department of Materials Science and Engineering, Korea University, Seoul 136-701, Korea.*
[b] *Materials Architecting Research Center, Korea Institute of Science and Technology, 39-1 Hawolgok-dong, Seongbuk-gu, Seoul 136-791, Korea.*
[c] *KIST-UNIST Ulsan Center for Convergent Materials, Ulsan National Institute of Science and Technology, Ulsan 689-698, Korea.*

† Electronic Supplementary Information (ESI) available: Experimental section; supporting figures (Fig. S1 – S14); supporting video for evaluation of the catalytic performance. See DOI: 10.1039/x0xx00000x

decoration with ultra-fine and uniform Pd NPs. This strategically well-tailored hybrid catalyst (Pd-PIBrGO) exhibits exceptional ultra-accelerated catalytic reduction of methylene blue (MB) to leuco methylene blue (LMB) in the presence of miniscule quantities of the hybrid catalyst, resulting in completion of the reaction in less than a few seconds.

The pyrene-functionalized ionic poly(dimethylaminoethyl methacrylate)-*b*-poly[poly(ethylene glycol) methyl ether methacrylate] (PDMAEMA-*b*-PPEGMEMA) block copolymer (PIB) (M_n: 19k, PDI: 1.09, 16 wt% of PDMAEMA, and 14 pyrene groups per chain) was synthesized by combination of atom transfer radical polymerization (ATRP) and a simple quaternization reaction, following the procedure outlined in Scheme S1. This PIB was functionalized with conjugated groups, cationic charges, and oxygen-rich organic functionalities to interconnect rGO and the Pd NPs, as well as to enhance the diffusion of positively charged reagents to the metal catalysts (Fig. 1a). The ionic block copolymer was applied to the functionalization of rGO by following the procedure in which rGO was mixed with PIB dispersed in NMP in a 1:4 ratio, followed by sonication and agitation. The free PIB was removed via simple filtration, and the obtained powdery products (polymer to rGO, 1:1) were redispersed in water (0.2 mg mL^{-1}). The formation of PIB-doped rGO (PIBrGO) is depicted in Fig. 1b. PIBrGO involved three distinct interactions (π–π, π–cation, and static), allowing for strong cohesion between PIB and rGO, along with the formation of an effective electron transfer path; the cationic charges and oxygen-rich PEGMEMA groups in the external layer of PIBrGO facilitated enhanced accessibility and adhesion of the Pd precursors and Pd NPs to the support, thus imparting enhanced dispersion stability to the composite (Fig. 1C).

The interfacial interactions between PIB and rGO were investigated by Raman and UV-Vis spectroscopy (Fig. 2A and B). The possible interfacial linkage forces are π–π, π–cation, and static interactions, arising from the pyrene-functionalized PDMAEMA block of PIB. These strong triple interactions can confer structural stability to the Pd-PIBrGO hybrid catalyst. The Raman spectrum of rGO exhibited predominant D and G bands at 1339.1 and 1582.8 cm^{-1}, corresponding to the sp^3 electronic configuration of disordered carbon bonds and the in-plane vibrations of sp^2 carbon bonds, respectively (Fig. 2A). Upon PIB adsorption, the D and G bands of rGO were shifted to higher wavenumber (1347.6 and 1586.5 cm^{-1}, respectively) because of the influence of electron transfer from rGO to PIB.[20,21] Evidence of this intermolecular energy transfer was obtained via UV-Vis spectroscopy. The PIB absorption spectrum in Fig. 2B exhibited characteristic peaks at 270.3, 279.3, 334.8, and 148.2 nm, attributed to pyrene moieties. After introduction of rGO, these absorption peaks were red-shifted by about 2 nm with peak broadening. This behavior can generally be explained in terms of the energy transfer effect, indicating good intercalation between rGO and PIB.[22-24]

The hybridization of PIBrGO with the Pd NPs was investigated by Raman spectroscopy. Pd NPs on the PIBrGO support can enhance the aforementioned electron transfer, resulting in a larger shift of the D and G bands of Pd-PIBrGO to higher wavenumber, i.e., 1349.4 and 1593.1 cm^{-1}, respectively. The D band to G band intensity ratio (ID/IG) of Pd-PIBrGO increased slightly from 1.01 to 1.05 in comparison to that of PIBrGO. A marginal decrease of the sp^2 domains can be induced by $NaBH_4$ reduction during hybridization.[25] Moreover, due to the electron transfer effect, the UV-Vis and Raman spectra of Pd-PIBrGO showed similar trends, exhibiting a slight red-shift with peak broadening in comparison to that of PIBrGO.

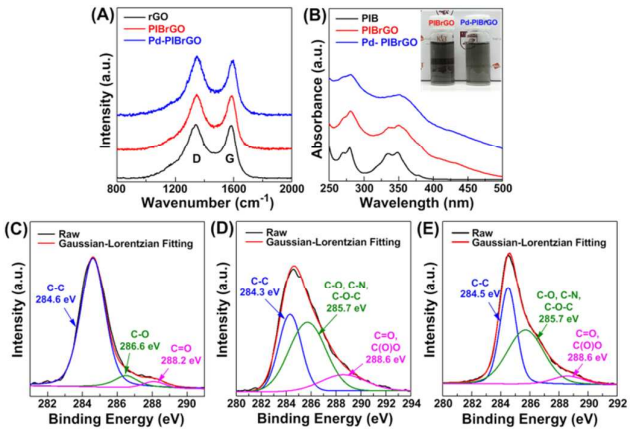

Fig. 2 (A) Raman spectra of rGO, PIBrGO, and Pd-PIBrGO. (B) UV-Vis. spectra of PIB, PIBrGO, and Pd-PIBrGO (inset: aqueous solutions of PIBrGO and Pd-PIBrGO). XPS spectra of (C) rGO, (D) PIBrGO, and (E) Pd-PIBrGO in the C 1s core-level region.

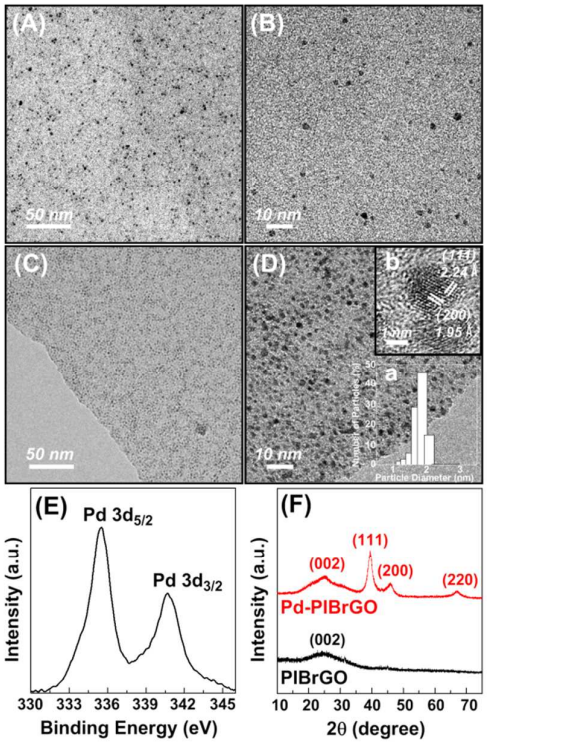

Fig. 3 TEM images of (A and B) Pd-rGO and (C and D) Pd-PIBrGO hybrid nanocomposites (D inset: a. size distribution of Pd NP, b. lattice-resolved TEM image of the Pd NP). (E) Pd 3d XPS spectrum of Pd-PIBrGO. (F) XRD patterns of PIBrGO and Pd-PIBrGO.

Additional characterizations of rGO, PIBrGO, and Pd-PIBrGO were performed by X-ray photoelectron spectroscopy (XPS) to investigate their surface elemental composition. The C 1s core-level spectra of rGO, PIBrGO, and Pd-PIBrGO are presented in Fig. 2C–E, respectively. The XPS C 1s spectrum of rGO can be deconvoluted into three peaks, corresponding to non-oxygenated carbon bonds at binding energies of 284.6 eV, C–O bonds at 286.6 eV, and C=O bonds at 288.2 eV (Fig. 2C). Compared with the binding energy of C 1s on the rGO surface, the PIBrGO spectrum provides evidence of the functionalization of rGO given that the intensity of the oxygenated carbon bonds predominantly increased and a new peak arising from the C–N bond appeared (Fig. 2D). This was ascribed to the presence of PIB on rGO, indicating that rGO was well-intercalated with PIB. After hybridization of PIBrGO with the Pd NPs, the peak originating from the C–C bonds (284.5 eV) showed the highest intensity, while the intensity of the peaks corresponding to the oxygenated carbon bonds was reduced (Fig. 2E). These results indicate reduction via $NaBH_4$ during the hybridization of PIBrGO with the Pd NPs.

The strategy for achieving dense decoration of well-dispersed, small-sized Pd NPs on the rGO surface involved the control via variation of the molar concentration of Na_2PdCl_4 from 2.5 mM to 20 mM. The effect of the hybridization conditions on formation of Pd NP-decorated PIBrGO was investigated by TEM (Fig. S6†). These TEM images showed that the target morphologies were achieved regardless of the Na_2PdCl_4 molar concentrations. However, deeper analysis of the TEM images showed mass aggregation with increasing Na_2PdCl_4 molar concentration, particularly for Pd NP-decorated PIBrGO obtained using 10 mM and 20 mM Na_2PdCl_4 (Fig. S7†). 5 mM Na_2PdCl_4 was optimal for hybridization of the PIBrGO with the Pd NPs. To evaluate the effects of PIB, TEM analysis of the hybridization of rGO and PIBrGO with the Pd NPs was undertaken (Fig. 3A–D), revealing that Pd NPs were well dispersed on the rGO support in Pd-rGO with a size distribution of 1–4 nm. Moreover, highly compact and well-dispersed decoration of uniform and small-sized Pd NPs (around 2 nm, Fig. 3D a) on the PIBrGO support was observed for Pd-PIBrGO despite the use of identical preparation procedures as applied for Pd-rGO.

Verification of the presence of Pd on the PIBrGO support was performed by X-ray studies. The Pd 3d XPS spectrum showed two typical peaks at 335.4 and 340.6 eV, which can be attributed to Pd $3d_{5/2}$ and Pd $3d_{3/2}$ of metallic Pd, respectively.[26] In addition, energy-dispersive X-ray (EDX) analysis of Pd-PIBrGO (Fig. S8†) confirmed the presence of Pd NPs on PIBrGO, as peaks arising from the Pd element were clearly found. Quantification of the EDX results indicated that Pd-PIBrGO was composed of 2.98% Pd, which is almost consistent with the XPS result (2.8%) obtained by quantification of the XPS survey spectrum (Fig. S9†). XRD was used to substantiate the formation of Pd-PIBrGO. The XRD spectrum of Pd-PIBrGO exhibited typical peaks at 39.4, 45.7, and 67.0°, respectively corresponding to the (111), (200), and (220) crystal planes of the face centered cubic (FCC) crystal structure of the Pd NPs. The additional peak at around 25° was

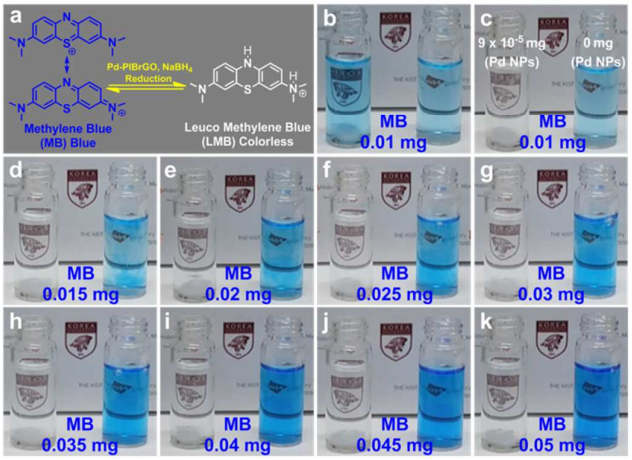

Fig. 4 Real-time photographs from the supporting video examining the sequential catalytic performance with and without Pd-PIBrGO. (a) Methylene blue reduction by NaBH4 in the presence of Pd-PIBrGO hybrid catalyst. (b) Initial solutions comprising of 2 mL (5 mg L^{-1}) of methylene blue and 1 mL (0.5 M) of NaBH4. (c) Photograph taken immediately following injection of 30 µL Pd-PIBrGO aqueous solution (0.1 mg mL^{-1}) into left vial. (d–k) Images of solutions with continual addition of 10 µL of methylene blue aqueous solution (500 mg L^{-1}) to both vials.

attributed to the (002) crystalline plane of the rGO support. The interplanar spacings of the (111) and (200) Pd NP lattices determined from the TEM image (Fig. 3D, inset b) were 2.24 Å and 1.95 Å, respectively. These results were consistent with the XRD results, which gave $d_{(111)}$ = 2.27 Å and $d_{(200)}$ = 1.98 Å. These X-ray studies indicated that Pd NPs were well-introduced on the PIBrGO support.

The catalytic activity of Pd-PIBrGO for the reduction of MB to LMB was examined as a probe reaction (Fig. 4a). The reduction mechanism on the surface of Pd NP can be addressed by the electron-transfer or electron relay system which occurred by an intermediate redox potential value of donor-acceptor (Fig. S12†).[27] The highly rapid catalytic reaction of Pd-PIBrGO and its recyclability were investigated using sequential reactions, as depicted in Fig. 4. We first prepared two solutions containing 2 mL (5 mg L^{-1}) of MB and 1 mL (0.5 M) of $NaBH_4$. Both solutions contained approximately 0.01 mg of MB; 30 µL of the Pd-PIBrGO (0.09 µg of Pd) hybrid catalyst was injected into only one MB solution (left). The solution was bleached to colorless by reduction of MB to LMB. The complete color change occurred within one second (Fig. 4c). This exceptionally rapid catalytic performance was shown to be operative after repeated injections (over 8 times) of 10 µL of MB solution (containing 0.005 mg of MB). In contrast, the color of the solution without the catalyst became increasingly blue with sequential additions of the MB solution. This interesting catalytic ability is derived from two morphological features of the Pd-PIBrGO hybrid catalyst: (1) the electronically negative oxygen-rich functional groups (PEGMEMA block in PIB) are end-deposited on the rGO surface, forming a brush-like structure. These groups can capture the positively charged reaction reagents (MB) owing to the static interactions and expedite it to the nearby catalyst; this facilitates diffusion of MB onto the electron-doped Pd NP surface much more rapidly

than the catalyst without PIB (Fig. S13†); (2) the size and formation of Pd NPs on the PIBrGO support also influenced their catalytic performance. The approximately 2 nm sized, uniform Pd NPs and highly compact

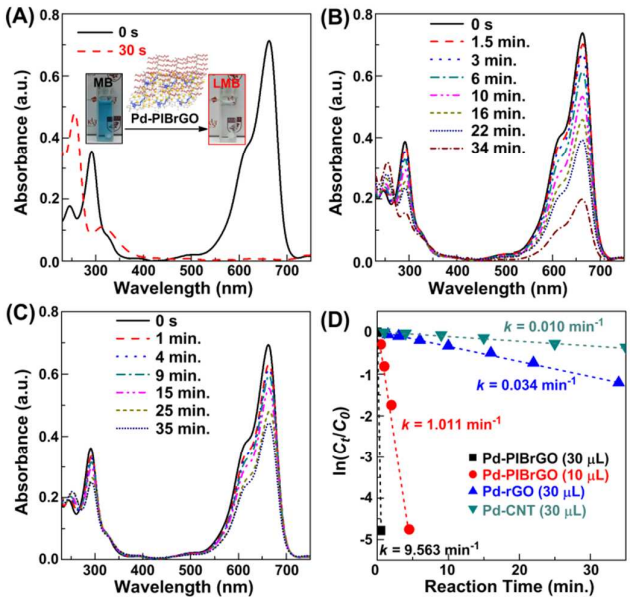

Fig. 5 Successive reduction reaction of methylene blue using 30 μL of (A) Pd-PIBrGO, (B) Pd-rGO, and (C) Pd-CNT aqueous solution (0.1 mg mL^{-1}). (D) $\ln(C_t/C_0)$ vs. reaction time (t) plots for Pd-PIBrGO, Pd-rGO, and Pd-CNT hybrid catalysts.

decoration with good dispersion stability provided an extremely large surface area and highly active edge and corner Pd atoms. Furthermore, the ionic block copolymer facilitated homogenous dispersion of the hybrid catalyst in aqueous solution, which can provide enhanced accessibility at the molecular level. These features made this hybrid catalyst well-optimized for the catalytic reaction, particularly for the positively charged reagents.

The reduction of MB to LMB was verified and monitored by UV-Vis spectroscopy. This reduction of MB by metal NPs is well-known to be able to produce LMB in the presence of $NaBH_4$, and has been generally used as a model reaction to examine the catalytic performance of newly developed catalysts.[28,29] To date, various types of catalysts have been introduced, such as single metals or alloys with unique structures, hybrid composite catalysts using carbons, polymers, or metal oxide supports, and metal-free catalysts.[30-33] However, application of the block copolymer with versatile functions, particularly involving the brush-like structure that functions to capture the free reagents in solution, to hybrid catalysts has not been reported so far. This is the inceptive study of the application of a pyrene-functionalized ionic block copolymer to the Pd-rGO hybrid catalyst to accelerate the catalytic activity.

The UV-Vis spectrum of MB exhibited a maximum absorption peak at 662.7 nm, corresponding to a blue color, and this peak gradually decreased with increasing reaction time after addition of the catalyst, while an adsorption peak emerged at 256 nm. With increasing reaction time, the color of the aqueous MB solution changed from blue to colorless, corresponding to the reduction of MB to LMB (Fig. 5A, inset). Based on the aforementioned reaction behavior, we evaluated the reduction of MB with various concentrations of the Pd-PIBrGO catalyst. The variation of the Pd-PIBrGO concentration was controlled from 10 μL (0.03 μg of Pd) to 100 μL (0.3 μg of Pd). Instant completion of the reduction reaction upon addition of the catalyst was achieved with the addition of 30 μL or more of the Pd-PIBrGO aqueous solution; MB reduction occurred instantaneously upon addition of the catalyst, evidenced by an immediate color change to colorless and complete disappearance of the UV absorption peak at 662.7 nm (Fig. 5A and supporting video). The minimum time for spectral acquisition with the UV-Vis spectroscopy system was around 30 sec. Thus, the reduction of MB in the presence of Pd-PIBrGO (Fig. 5A) may be much faster than measured. However, two reference catalysts (Pd-rGO and Pd-CNT) did not produce immediate reduction of MB under the same conditions used for Pd-PIBrGO, as shown in Fig. 5B and C, respectively.

Pseudo first order reaction kinetics was applied to determine the reaction rate constant for the reduction of MB, which can be normalized to the equation:

$$\ln(C_t/C_0) = -kt \quad (1)$$

where C_t is the concentration of MB at time t, C_0 is the initial concentration of MB, and k is the pseudo-first order rate constant.[34] Fig. 5D shows the $\ln(C_t/C_0)$ vs. t plots for Pd-PIBrGO, Pd-rGO, and Pd-CNT. The plots were all linear, in good agreement with the pseudo-first order kinetic model. From Eq. (1), the rate constants for the Pd-PIBrGO (30 μL), Pd-rGO (30 μL), and Pd-CNT (30 μL) systems were calculated to be about 9.563, 0.034, and 0.01 min^{-1}, respectively (Fig. 5D). The rate constant for the two dimensional Pd-rGO system was 3-fold higher than that of the one dimensional Pd-CNT system for composites with similar Pd content (1.01%), indicating that the support-effect influenced the MB adsorption capability of the catalyst. Moreover, the rate constant achieved with the Pd-PIBrGO hybrid catalyst was exceptionally high, being over 280-fold higher than that achieved with Pd-rGO. This can be attributed to three factors: (1) the morphologically tailored Pd embellishment on PIBrGO provided a considerably large surface area and over 3-fold more Pd NPs on the support than Pd-rGO, (2) the presence of PIB as a diffusion agent led to much more effective delivery of MB molecules onto the active Pd metals, facilitating accelerated catalysis, (3) the better dispersion stability of Pd-PIBrGO in the aqueous solution facilitated better accessibility of the reagents to the catalyst. Furthermore, although we reduced the quantity of the Pd-PIBrGO hybrid catalyst used in the reduction of MB to 10 μL (0.03 μg of Pd), the rate constant remained very high at about 1.011 min^{-1} (Fig. S14†), which was still 30-fold higher than that of Pd-rGO (30 μL). To the best of our knowledge, this catalytic ability of Pd-PIBrGO is superior to and much more effective than that of recently reported catalysts.[28,29,36,37] The further evaluation for the catalytic activity of Pd-PIBrGO was

performed by calculation of the turnover frequency (TOF, defined as the moles of MB molecules per moles of Pd catalyst per minute), resulting in TOF = 2198.4 mol mol^{-1} min^{-1}. This TOF value strongly indicated its greater catalytic performance in the reduction of MB than in previously reported systems, including tetrahedral Pd nanocrystals (TOF = 0.38 mol mol^{-1} min^{-1}),[38] tetrahedral Pd nanocrystals supported by graphene (TOF = 1.2 mol mol^{-1} min^{-1}),[38] platinum NP-decorated rGO (TOF = 7.1 mol mol^{-1} min^{-1}),[39] and Fe_3O_4-Pt decorated rGO (TOF = 18.5 mol mol^{-1} min^{-1}).[39] To confirm the structural stability of Pd-PIBrGO, TEM analysis was performed after performing 10-times catalytic reactions with methylene blue (Fig. S15†), indicating that the morphology of Pd-PIBrGO was maintained albeit sequential catalytic reactions were performed.

The catalytic activity of Pd-PIBrGO with regard to negatively charged reaction reagents was also considered. Another model reaction employing 4-nitrophenol (4-NP), which is a well-known probe reaction material exhibiting a color change from yellow to colorless after reduction to 4-aminophenol (4-AP), was evaluated (Fig. S16†).[4,19,28,33,40-42] The results of catalytic reduction of 4-NP using Pd-PIBrGO and Pd-rGO are depicted in Fig. S17†. The rate constant for the Pd-PIBrGO (100 μL) system was lower (2.239 min^{-1}) than that obtained in the previous model reaction, even when a 3-fold higher quantity of the Pd-PIBrGO hybrid catalyst was used. This difference in the catalytic performance can be explained by curtailment of the acceleration-effect in the Pd-PIBrGO hybrid catalyst. However, the rate constant achieved with Pd-PIBrGO was still 13-fold higher than that obtained with Pd-rGO (100 μL) (0.165 min^{-1}), indicating the superior catalytic performance of Pd-PIBrGO even with the use of negatively charged reagents.

Conclusions

We developed a rationally designed PIB-doped rGO (PIBrGO) support based on four design features: (1) structural stability by strong adhesion, (2) good facilities for the compact decoration of approximately 2 nm sized Pd NPs, (3) effective electron transfer, (4) facilitated diffusion of the reagents to the metal catalysts for accelerated catalytic performance. We obtained exceptionally advanced catalytic performance in the reduction of MB to LMB using miniscule quantities of the Pd-PIBrGO hybrid catalyst (0.09 μg of Pd), resulting in completion of the reaction in less than a few seconds, and achieved over 280-fold increase of the reaction rate constant (k = 9.563 min^{-1}) in comparison to Pd-rGO (k = 0.034 min^{-1}). This surprisingly effective catalytic performance was retained over several sequential additions of 10 μL MB (500 mg L^{-1}) (see the supporting video).

Acknowledgements

This work was supported by the Industrial Strategic Technology Development Program (Project No. 10041829, Development of Prototype 154 kV Compact Power Cables with Insulation Thickness Decreased by 15% or More Based on Ultra-super Smooth Semiconductive Materials) funded by the Ministry of Trade, Industry & Energy (MI, Korea) and partially supported by the KIST-UNIST Partnership Program.

References

1 T. Yasukawa, H. Miyamura and S. Kobayashi, *Chem. Soc. Rev.,* 2014, **43**, 1450.
2 H. Li, J. V. John, S. J. Byeon, M. S. Heo, J. H. Sung, K. –H. Kim and I. Kim, *Prog. Polym. Sci.,* 2014, **39**, 1878.
3 W. Yu, M. D. Porosoff and J. G. Chen, *Chem. Rev.,* 2012, **112**, 5780.
4 T. Aditya, A. Pal and T. Pal, *Chem. Commun.,* 2015, **51**, 9410.
5 D. S. Su, S. Perathoner and G. Centi, *Chem. Rev.,* 2013, **113**, 5782.
6 M. Kaushik, K. Basu, C. Benoit, C. M. Cirtiu, H. Vali and A. Moores, *J. Am. Chem. Soc.*, 2015, **137**, 6124.
7 C. J. Shearer, A. Cherevan and D. Eder, *Adv. Mater.*, 2014, **26**, 2295.
8 H. Huang, S. Yang, R. Vajtai, X. Wang and P. M. Ajayan, *Adv. Mater.*, 2014, **26**, 5160.
9 H. Bai, C. Li and G. Shi, *Adv. Mater.*, 2011, **23**, 1089.
10 X. Zhou, J. Qiao, L. Yang and J. Zhang, *Adv. Energy Mater.*, 2014, **4**, 1301523.
11 B. Cai, X. Lv, S. Gan, M. Zhou, W. Ma, T. Wu, F. Li, D. Han and L. Niu, *Nanoscale*, 2013, **5**, 1910.
12 Y. Liang, Y. Li, H. Wang, J. Zhou, J. Wang, T. Regier and H. Dai, *Nat. Mater.*, 2011, **10**, 780.
13 J. Liu, S. Fu, B. Yuan, Y. Li and Z. Deng, *J. Am. Chem. Soc.*, 2010, **132**, 7279.
14 M. –Y. Wang, T. Shen, M. Wang, D. –E, Zhang, Z. –W. Tong and J. Chen, *Sens. Actuators, B*, 2014, **190**, 645.
15 H. Wang, D. Zhang, T. Yan, X. Wen, L. Shi and J. Zhang, *J. Mater. Chem.,* 2012, **22**, 23945.
16 H. Wang, D. Zhang, T. Yan, X. Wen, J. Zhang, L. Shi and Q. Zhong, *J. Mater. Chem. A,* 2013, **1**, 11778.
17 Y. Yokomizo, S. Krishnamurthy and P. V. Kamat, *Catal. Today*, 2013, **199**, 36.
18 H. Wang, L. Shi, T. Yan, J. Zhang, Q. Zhong and D. Zhang, *J. Mater. Chem. A,* 2014, **2**, 4739.
19 H. Li, L. Han, J. J. Cooper-White and I. Kim, *Nanoscale*, 2012, **4**, 1355.
20 S. Wang, D. Yu, L. Dai, D. W. Chang and J. –B. Baek, *ACS Nano*, 2011, **8**, 6202.
21 A. M. Rao, P. C. Eklung, S. Bandow, A. Thess and R. E. Smalley, *Nature*, 1997, **388**, 257.
22 Y. Min, G. Q. He, Q. J. Xu and Y. C. Chen, *J. Mater. Chem. A*, 2014, **2**, 1294.
23 K. Y. Cho, Y. S. Yeom, H. Y. Seo, Y. H. Park, H. N. Jang, K. –Y. Baek and H. G. Yoon, *ACS Appl. Mater. Interfaces*, 2015, **7**, 9841.
24 V. Skrypnychuk, N. Boulanger, V. Yu, M. Hilke, S. C. B. Mannsfeld, M. F. Toney and D. R. Barbero, *Adv. Funct. Mater.*, 2015, **25**, 664.
25 I. K. Moon, J. Lee, R. S. Ruoff and H. Lee, *Nat. Commun.*, 2010, **1**, 73.
26 S. –I. Yamamoto, H. Kinoshita, H. Hashimoto and Y. Nishina, *Nanoscale*, 2014, **6**, 6501.
27 H. Hu, M. Shao, W. Zhang, L. Lu, H. Wang and S. Wang, *J. Phys. Chem. C,* 2007, **111**, 3467.
28 A. Ma, Y. Xie, J. Xu, H. Zeng and H. Xu, *Chem. Commun.*, 2015, **51**, 1469.
29 T. Yao, T. Cui, H. Wang, L. Xu, F. Cui and J. Wu, *Nanoscale*, 2014, 6, 7666.
30 D. Wang and Y. Li, *Adv. Mater.*, 2011, **23**, 1044.
31 H. Huang and X. Wang, *J. Mater. Chem.,* 2014, **2**, 6266.

32 W. Zhang, Y. Liu, G. Lu, Y. Wang, S. Li, C. Cui, J. Wu, Z. Xu, D. Tian, W. Huang, J. S. DuCheneu, W. D. Wei, H. Chen, Y. Yang and F. Huo, *Adv. Mater.*, 2015, **27**, 2923.
33 J. He, W. Ji, L. Yao, Y. Wang, B. Khezri, R. D. Webster and H. Chen, *Adv. Mater.*, 2014, **26**, 4151.
34 J. Huang, Y. Zhu, M. Lin, Q. Wang, L. Zhao, Y. Yang, K. X. Yao and Y. Han, *J. Am. Chem. Soc.*, 2013, **135**, 8552.
35 J. W. Lekse, B. J. Haycock, J. P. Lewis, D. R. Kauffman and C. Matranga, *J. Mater. Chem. A*, 2014, **2**, 9331.
36 Y. Zhao, C. Eley, J. Hu, J. S. Foord, L. Ye, H. He and S. C. E. Tsang, *Angew. Chem. Int. Ed.*, 2012, **51**, 3846.
37 O. Yehezkeli, D. R. B. de Oliveira and J. N. Cha, *Small*, 2015, **11**, 668.
38 G. Fu, L. Tao, M. Zhang, Y. Chen, Y. Tang, J. Lin and T. Lu, *Nanoscale,* 2013, **5**, 8007.
39 S. Wu, Q. He, C. Zhou, X. Qi, X. Huang, Z. Yin, Y. Yang and H. Zhang, *Nanoscale*, 2012, **4**, 2478.
40 X. Zhang and Z. Su, *Adv. Mater.*, 2012, **24**, 4574.
41 W. Zhang, G. Lu, C. Cui, Y. Liu, S. Li, W. Yan, C. Xing, Y. R. Chi, Y. Yang and F. Huo, *Adv. Mater.*, 2014, **26**, 4056.
42 J. Zhou, B. Duan, Z. Fang, J. Song, C. Wang, P. B. Messersmith and H. Duan, *Adv. Mater.*, 2014, **26**, 701.

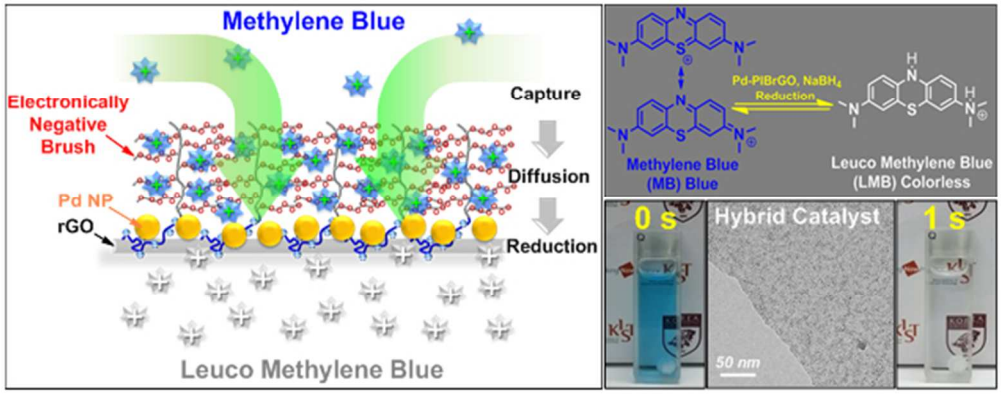

168x66mm (96 x 96 DPI)